Extracting Multi-Person Respiration from Entangled RF Signals

SHICHAO YUE, Massachusetts Institute of Technology
HAO HE, Massachusetts Institute of Technology
HAO WANG, Massachusetts Institute of Technology
HARIHARAN RAHUL, Massachusetts Institute of Technology
DINA KATABI, Massachusetts Institute of Technology

Recent advances in wireless systems have demonstrated the possibility of tracking a person's respiration using the RF signals that bounce off her body. The resulting breathing signal can be used to infer the person's sleep quality and stages; it also allows for monitoring sleep apnea and other sleep disordered breathing (SDB); all without any body contact. Unfortunately however past work fails when people are close to each other, e.g., a couple sharing the same bed. In this case, the breathing signals of nearby individuals interfere with each other and super-impose in the received signal.

This paper presents DeepBreath, the first RF-based respiration monitoring system that can recover the breathing signals of multiple individuals even when they are separated by zero distance. To design DeepBreath, we model interference due to multiple reflected RF signals and demonstrate that the original breathing can be recovered via independent component analysis (ICA). We design a full system that eliminates interference and recovers the original breathing signals. We empirically evaluate DeepBreath using 21 nights of sleep and over 150 hours of data from 13 couples who share the bed. Our results show that DeepBreath is very accurate. Specifically, the differences between the breathing signals it recovers and the ground truth are on par with the difference between the same breathing signal measured at the person's chest and belly.

CCS Concepts: • **Human-centered computing** → *Ubiquitous and mobile computing systems and tools*;

Additional Key Words and Phrases: Multi-Person Respiration Monitoring, Wireless Sensing, Blind Source Separation, Full-Night Monitoring

1 INTRODUCTION

Breathing is an important health metric used for tracking diseases in many areas, such as sleep [27, 37], pulmonology [30], and cardiology [7, 47]. It can also provide useful insights about the psychological state of an individual [19, 20]. Respiration monitoring during sleep is particularly useful. For example, the respiration signal can be used to infer the person's sleep stages (light, deep or REM sleep) [22, 40, 49] and diagnose sleep disorders [4, 12]. Monitoring can also be used to track sleep disturbed breathing (SDB) which has been associated with

Correspondence to: Shichao Yue <scyue@mit.edu>.
Authors' addresses: Shichao Yue, Massachusetts Institute of Technology, scyue@mit.edu; Hao He, Massachusetts Institute of Technology, haohe@mit.edu; Hao Wang, Massachusetts Institute of Technology, hwang87@mit.edu; Hariharan Rahul, Massachusetts Institute of Technology, rahul@csail.mit.edu; Dina Katabi, Massachusetts Institute of Technology, dina@csail.mit.edu.

cardiac arrest in heart failure patients [25, 46]. Furthermore, respiration monitoring is important for diagnosing and tracking sleep apnea, a condition in which the person stops breathing for short intervals during the night [6].

Traditional approaches for respiration monitoring are relatively cumbersome. They require the person to wear a breathing belt and/or a nasal probe and sleep with it. However, recent advances in RF-based sensing have demonstrated the possibility of monitoring breathing without any sensor on the person's body [2, 14, 31]. Such systems transmit a low power wireless signal and capture its reflections. The signal bounces off the people in the environment and gets modulated by their breathing. The receiver uses the reflected signal to track the person's breathing without any sensors on the body.

However, past work on RF-based respiration monitoring requires monitored people to be located away from each other. This requirement precludes respiration monitoring during sleep for people who share the same bed. Hence, it prevents a large fraction of the population benefiting from such technology including couples that share the same bed, and new mothers who sleep with their infants.

Tracking respiration when people are next to each other is a difficult problem. RF reflections off two bodies super-impose (i.e. add up) over the wireless medium and interfere at the receiver. For relatively distant people, one can use antenna arrays and/or Frequency-Modulated Continuous Wave (FMCW) radios [23] to zoom in on the location of a particular individual and receive the signal reflected off his/her body with limited to no interference. However, as people get closer, interference becomes too high. Hence, even systems that combine antenna arrays and FMCW still require a minimum separation of 1.5 to 2 meters [2, 14]. Fundamentally, today there is no solution that can disentangle mixed RF-based breathing signals. Hence, all systems require a minimum distance between monitored users.

This paper introduces DeepBreath, the first system that disentangles mixed RF-based breathing signals. DeepBreath can monitor the respiration signals of multiple people even if they have zero distance between them. It also provides continuous monitoring throughout the night for people who share the same bed.

The design of DeepBreath combines three components as described below.

(a) Breathing Separation: DeepBreath has a breathing separation module that reconstructs the correct breathing signals of multiple co-located individuals. To design this component, we first model how RF-based breathing signals mix over the wireless medium. We show that the mixing is complicated by changes in the wireless channels due to movements. We present an approximation that allows us to formulate the problem as blind source separation and solve it using independent component analysis (ICA). Given this new formulation, DeepBreath uses an FMCW radio equipped with an antenna array to zoom in on RF signals from different locations in space. It calls those RF signals observations. DeepBreath uses its formulation of the mixing process to recover the original breathing signals from such observations using ICA.

(b) Motion Detection: When people move, their location changes and the contribution of their breathing to each observation changes. Hence the mapping from observations to original breathing signals has to be recomputed. Note that even a small motion – such as turning in bed – changes the mapping. Thus, DeepBreath has to automatically detect such movements and run its breathing separation module on each stable period separately. To detect motion reliably DeepBreath uses a convolutional neural network that is trained to identify movements of the monitored people and ignore irrelevant motion, e.g, a fan or the HVAC (Heating, ventilation and air conditioning).

(c) Identity Matching: For continuous monitoring, a night of sleep has to be segmented into multiple periods of stable breathing with no motion. Yet, when running ICA on each such period, the recovered breathing signals can be permuted in the output. For example, say there are 2 people in the environment. During the first period, the first ICA component may refer to the first person's breathing and the second component to the second person's breathing. However, in the next period, the situation may flip. How do we identify the ICA components that correspond to the breathing of the same individual in different periods? We formulate this problem as an optimization problem, where the solution maximizes a similarity metric between the person's breathing signals
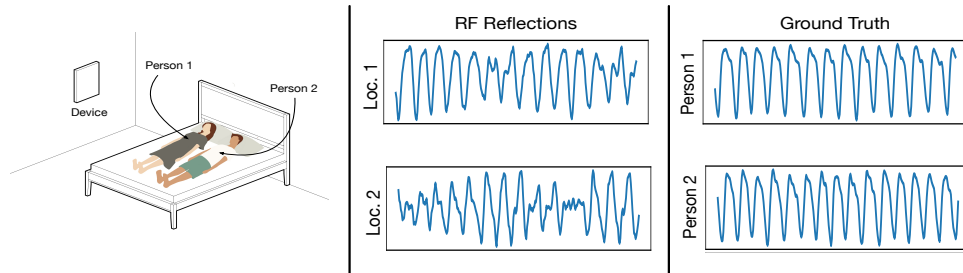
Fig. 1. A scenario of two people sharing a bed. Loc. 1 and Loc. 2 represent the locations of Person 1 and Person 2's bodies. During this moment, both Person 1 and Person 2 are breathing normally, yet the reflected signal from Loc. 2 indicates Person 2 has an apnea event.

across different periods. We solve this optimization using dynamic programming. The final solution provides a robust system that disentangles the breathing signals of multiple people and delivers continuous respiration monitoring throughout the night.

We have implemented DeepBreath and evaluated it with 13 couples.[1] The couples sleep in the same bed, with the bed size ranging from twin (1m wide) to king (2m). To obtain ground truth breathing, each subject sleeps with an FDA-approved respiration monitoring belt [36]. In total, we have collected 21 nights of sleep, and 151 hours of data. To measure the accuracy of the reconstructed breathing signal, we compute its correlation with the ground truth signal from the respiration belt. Note that the correlation between two breathing belts on the same subject, one on the chest and one on the belly is around 0.915. Thus a comparable correlation value indicates a high accuracy of the recovered breathing signals.

Our experiments show that DeepBreath recovers the breathing signals of couples sharing the bed with high accuracy. Specifically, the recovered breathing signal has an average correlation of 0.914 with the breathing belt signal measured on the subject's chest. DeepBreath also recovers the breathing rates of the monitored subjects with an average error as small as 0.140 breaths per minute.[2]

Further, DeepBreath scales beyond two people. We conduct experiments with 5 subjects sitting shoulder-to-shoulder on one couch. DeepBreath can recover the breathing signals of all 5 subjects with an average correlation of 0.922 with the ground truth breathing signals.

To the best of our knowledge, this is the first paper that demonstrates a system that recovers the detailed respiration signals of multiple people sharing the bed or sitting with zero separation. This result renders much recent research using RF signals to monitor respiration, sleep, and apnea applicable to a significantly larger segment of the population including couples sharing the same bed and recent mothers sleeping with their babies.

2 ILLUSTRATIVE EXAMPLE

Consider a scenario in which a couple shares the bed. Let us examine the accuracy of monitoring their breathing using the state of the art RF techniques. To do so, we use an FMCW radio equipped with an antenna array as in [2]. Such a radio divides the space into voxels, and separates RF signals received from different spatial voxels. We deploy the radio in the couple's bedroom as shown in the first column in Fig. 1. We also ask both subjects to wear a respiration belt to obtain their ground truth breathing.

---

[1] All experiments are approved by our IRB.

[2] Average breathing rate of all the subjects is 15.68 breaths per minute, with a standard deviation of 2.18 breaths per minute. So our system's breathing rate percentage error is 0.89%.

We measure the exact location of both subjects with respect to the radio using the Bosch GLM50 laser distance measurement tool [5]. We then make the FMCW radio and antenna array zoom in on the two voxels in space that are centered on the chest of each subject. This gives us the best estimates of the subjects' breathing signals based on past work, under the assumption that past work is able to perfectly localize the subjects. We plot those RF signals in the middle column in Fig. 1. The figure shows that by looking at RF reflections from the two subjects, it seems that person 2 has experienced an apnea event – i.e., a period during which he did not breath.

Now let us look at the actual breathing signals from the two belts on the subjects, which we show in the third column in Fig. 1. The ground truth shows that both subjects have regular breathing and neither of them had an apnea event, which contradicts the behavior shown in the RF signals reflected off their chests. This can lead to serious errors in reporting a person's health condition.

This experiment shows that even if one zooms in on the signal from the exact location of the person's chest, one cannot eliminate the effect of the signal reflected off a nearby person. The reason we cannot completely separate the two signals is that antenna arrays and FMCW are filters over space. However, no filter is perfect. In particular, both antenna arrays and FMCW filter signals using the Fourier transform [1, 23]. Since the Fourier transform is applied over a finite window, it will result in a *sinc* in the frequency domain. This causes nearby signals to mix with each other due to the sinc tail, as shown in Fig. 2. The closer the two people are, the closer the frequency response after taking the Fourier Transform, and the more the corresponding sinc functions leak into each other.

(a) Two sine waves with different frequency   (b) Windowed Fourier Transform result
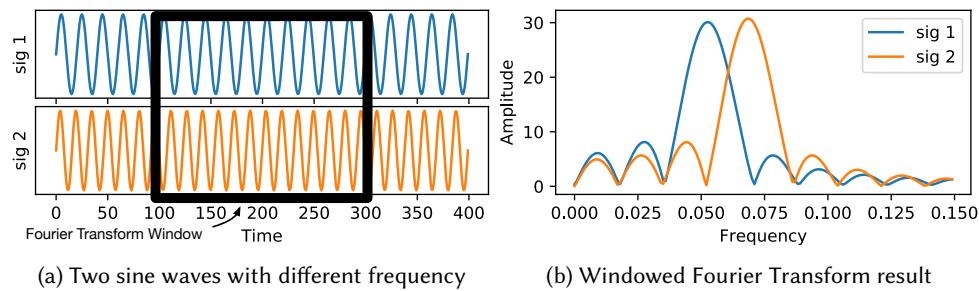
Fig. 2. A sinc example. Fig. 2a shows two sine waves with slightly different frequency. The black box on top of the signals indicates the Fourier Transform window. Fig. 2b shows the result of the Fourier Transform. The two signals are sincs in frequency domain, and when the frequencies of the signals are similar, their sincs are close to each other.

3 RELATED WORK

Our work is related to past work on RF-based sensing and the general literature on blind source separation.

3.1 RF-Based Sensing

Recent years have witnessed much interest in using RF signals to monitor people's movements and vital signs without any on-body sensors. Researchers have developed systems that transmit low power RF signal and monitor its reflections. They used these reflections to infer a person's location [1, 18], gait [15, 44], breathing [2, 9, 14, 43], heart rate [2, 9] and even emotions [48].

Our work is closest to past work that uses RF signals to monitor breathing. Studies using Doppler Radar [31], FMCW [2, 14, 49], millimeter waves [9, 45], and WiFi signals [21, 43] all demonstrate accurate monitoring of a single person's breathing. Respiration monitoring using radio signal is also closely related to monitoring breathing using acoustic signals, which tends to use FMCW techniques and demonstrates good accuracy for a

single person [26, 41]. Further, some recent papers demonstrate that the breathing signal extracted from RF can be used to infer additional health metrics [34, 48]. In particular, a larger number of papers use the breathing extracted from RF to monitor sleep quality, track insomnia, and infer sleep stages [14, 21, 31, 49].

A key challenge in passive wireless monitoring is the interference between different people. RF signals reflect off all people in the environment. Those reflections super-impose over the wireless medium and add-up in the received signal. To avoid this problem, much of the past work assumes a single person in the environment [1, 48, 49]. Papers that show results for multiple users require people to have a minimum separation of 1.5 to 2 meters [2, 14, 45]. Having a minimum separation between subjects reduces the mixing between the RF signals reflected off their bodies, and allows the receiver to zoom in on each individual using techniques like FMCW and antenna arrays. The need for such minimum separation prevents past work from monitoring users sitting next to each other or sleeping in the same bed. The only past studies, that we know of, that report breathing results for users in the same bed are [43] and Nandakumar et al. [26]. The former requires the users to lie in a specific position and have significantly different breathing rates. The latter uses audio signals as opposed to RF signals, and hence is vulnerable to environmental audio sources and is affected by thick comforters and clothes. Furthermore, both studies only report the breathing rate, which is an average value over a long interval. Recovering the exact details of the breathing signal is a much more demanding task.

More fundamentally, all past work relies on the existence of good RF/audio signals that do not suffer from interference and mixing, and no past work can disentangle multiple breathing signals when they are mixed together. In contrast, by modeling different reflections of FMCW as linear combinations of breathing signals, and applying independent component analysis, our system can disentangle breathing signals from mixtures of such signals. Hence, it can accurately monitor multiple users' respiration signals without a minimum separation requirement.

3.2 Blind Source Separation and Independent Component Analysis (ICA)

DeepBreath leverages the literature on blind source separation (BSS) [8]. The problem is defined as the recovery of a set of source signals from a set of mixture signals, without knowing the properties of the original sources or how they are mixed together. If the sources are independent and have non-Gaussian distributions, and the mixing is linear, then one can use independent component analysis (ICA) to recover the source signals from the mixture signals. ICA recovers the original sources by maximizing the statistical independence of the estimated components in the mixtures [16, 17].

ICA has been used in many domains including speech and image processing, text mining, financial data processing, communication systems, and EEG processing [11, 24, 28, 33, 38, 39]. In this paper, we extend the applications of ICA to include the recovery of the breathing signals of collocated individuals.

4 MODELING MIXTURES OF RF-BASED BREATHING SIGNALS

In this section, we discuss how to separate mixtures of RF breathing signals.

4.1 Primer

Breathing signals have a variety of patterns that are unpredictable in advance, and the results of multiple people breathing in an environment are seen in a combined form in the observed RF signals. Identifying the individual breathing signals from the combined RF signals falls under the broad framework of *Blind Source Separation*. A common example of such blind source separation is the *cocktail party problem*, where the audio signals from multiple speakers are combined in the environment, and the goal is to separate the audio signals corresponding to each individual speakers. In the particular case that the sources are independent, non-Gaussian, and combine

linearly, we can perform Blind Source Separation efficiently using a technique called *Independent Component Analysis (ICA)*.

Traditionally, ICA is defined as follows: Let there be N independent time varying sources, $s_i(t), i = 1 \ldots N$, and M different observations, $x_i(t), i = 1 \ldots M$. For T time units ($t = 1 \ldots T$), we can define the source signals as a $N \times T$ matrix,

$$S_{N \times T} = \begin{bmatrix} s_{11} & s_{12} & \cdots \\ \vdots & \ddots & \\ s_{N1} & & s_{NT} \end{bmatrix}$$

and the observations as a $M \times T$ matrix,

$$X_{M \times T} = \begin{bmatrix} x_{11} & x_{12} & \cdots \\ \vdots & \ddots & \\ x_{M1} & & s_{MT} \end{bmatrix}$$

The observations X are produced by the sources S combining via a mixing matrix $W_{M \times N}$, such that we can write:

$$X_{M \times T} = W_{M \times N} \times S_{N \times T} \tag{1}$$

The goal of ICA is to recover the sources S and the mixing matrix W given only the observations X, provided the sources are independent and non-Gaussian.

4.2 The Challenge in Applying ICA to RF Breathing

At first blush, it might seem that applying ICA to recover mixed breathing signals is simple. The RF signals reflected off people's bodies add up linearly over the wireless medium. Further, the breathing signals of different subjects are generally independent and not Gaussian.[3] The problem, however, is that Eq. 1 assumes that the mixing matrix W is the same at every time instance. ICA leverages the distribution of the sources during the period T to impose additional constraints to solve the problem. Unfortunately, this assumption does not hold for our problem.

In our problem, the sources are the RF signals reflected off each person's torso. At any point in time, antennas on the radio receive linear mixtures of these reflections. The mixing coefficients, W, are the wireless channels from the torso of each person to each antenna. When the person breathes, his/her torso moves. As a result, the channels change and the mixing coefficients are no longer constant. This means that there is not a single mixing matrix that can be used independent of time in Eq. 1.

In the remaining parts of this section, we describe the mathematical structure of the RF signal, how the signal changes with multiple reflectors, and how we can reformulate the mixing problem to allow source identification using ICA.

4.3 FMCW with a Single Reflector

We will analyze RF reflections assuming a Frequency-Modulated Carrier Waves (FMCW) radio, which is widely used in the literature [2, 14, 49]. FMCW operates by transmitting a sequence of sweeps. During each sweep, the frequency of the transmitted signal changes linearly with time, as illustrated by the red lines in Fig. 3. The human body reflects the signal back. The reflected signal, depicted in blue, is a time-shifted version of the transmitted sweep, where the shift is equal to the time it takes the signal to travel to the reflector and back to the radio. Because the duration of each sweep is usually very short ($\sim 0.1ms$), we assume the reflector does not move within each sweep. For a single reflector at distance $d(t)$ during the tth sweep, the signal's time-in-flight is

---

[3]In the evaluation section, we show the distribution of a person's breathing signal.
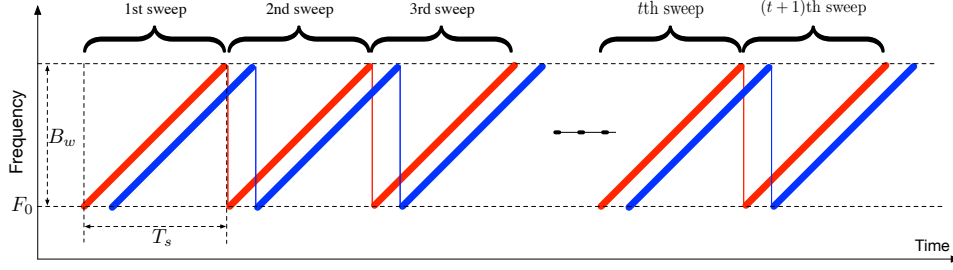
Fig. 3. Transmitted and received FMCW signal. The red line is the transmitted signal, and the blue line is the received signal reflected by a single reflector. FMCW operates by transmitting a sequence of sweeps, and comparing the frequency difference between the transmitted signal and received signal.

$\tau(d(t)) = 2d(t)/C$, where C is the speed of light. In this case, the received FMCW signal within the tth sweep can be written in the time domain as [29]:

$$m(d(t), u) = Ae^{j2\pi(F_0\tau(d(t))+K_s\tau(d(t))u-1/2K_s\tau^2(d(t)))}, u \in [0, T_s],$$ (2)

where A is the amplitude of the received signal, F_0 is the smallest frequency in the sweep, T_s is the *sweeping period*, and $K_s = B_w/T_s$ is sweeping rate defined as the swept bandwidth divided by the sweeping time. For convenience, we also define the following quantities: *carrier-to-bandwidth ratio* $R = F_0/B_w$, and *resolution* $U = C/2B_w$.

In order to compute the frequency response of this time domain signal, we can compute the Fourier Transform of the signal within each sweep. We leave the details of the derivation to appendix A, and summarize the final result here. The frequency response at a subcarrier f for a reflector at distance $d(t)$ can be written as:

$$l(d(t), f) = h(f) \cdot sinc(v(d(t), f))e^{2\pi j(R+1/2)v(d(t),f)}$$ (3)

where $h(f) = AT_se^{k2\pi Rf}$ and $v(d(t), f) = \frac{d(t)}{U} + fT_s$.

4.4 FMCW with Multiple Reflectors

Now consider the case with multiple reflectors $r_1, r_2, \ldots, r_N$, at distances $d_1, d_2, \ldots, d_N$. In such a case, the total reflected signal for the N reflectors is simply the sum of the corresponding time domain signals, *i.e.*, $M(t, u) = \sum_{i=1}^{N} m(d_i(t), u)$.

Since Fourier Transform is linear, the frequency domain representation of $M(t)$ can be obtained simply by summing the individual frequency distributions, *i.e*

$$L(d(t), f) = \sum_{i=1}^{N} l(d_i(t), f).$$ (4)

As can be seen from Eq. 3, the function $L(d(t), f)$ can no longer be written as a linear sum of N independent sources, *i.e.*, one cannot define sources $g(d_1(t)), \ldots, g(d_N(t))$ (note that $g(.)$ are not a function of frequency f) such that we can write the output signal

$$L(d(t), f) = \sum_{i=1}^{N} w_i(f)g(d_i(t)),$$ (5)

for every f, where the $w_i(f)$ are the mixing coefficients and remain constant for all the sweeps. This prevents us from directly applying ICA to the signal $L(d(t), f)$, as described in §4.2.
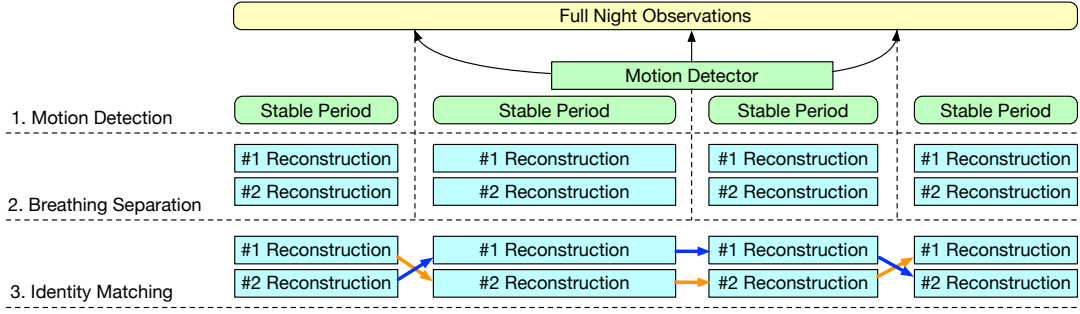
Fig. 4. The architecture of DeepBreath. DeepBreath has three components: a motion detector to detect motions disruptive to ICA and generate stable periods, a breathing separation module that adapts ICA to recover breathing signal candidates, and an identity matching module to stitch all reconstructed breathing signals that belong to the same person.

4.5 Making ICA Work for FMCW with Multiple Reflectors

Our key insight, however, is that we can create such a decomposition by considering only the small linear motions involved with breathing. Specifically, we can write $l(d_i(t), f)$ as $l(D_i + \delta_i(t), f)$ where D_i is the mean position of the reflector (i.e., the mean position of the chest during breathing), and $\delta_i(t)$ are the small time varying motions corresponding to breathing. Using the Taylor series expansion till the first order term, this function can be approximated as: $l(d_i(t), f) = l(D_i, f) + \delta_i(t)l'(D_i, f)$, where $l'(D_i, f)$ is the derivative with respect to distance. The total frequency response for all the N reflectors can then be written as:

$$L(d(t), f) = \sum_{i=1}^{N} l(D_i, f) + \sum_{i=1}^{N} l'(D_i, f)\delta_i(t) \tag{6}$$

In Eq. 6, note that the first term is simply the mean frequency response across all time units, which we can subtract from the signal without affecting the estimation of the breathing signal. The second term is exactly of the form in Eq. 5 desired by ICA, where the derivative term corresponds to the desired ICA mixing coefficient, and the $\delta_i(t)$ corresponds to the time varying source relevant to the breathing motion.

Thus, we can apply ICA algorithms to this modified signal, *i.e.* after subtracting the mean across time for each frequency and recover the individual breathing motions of all the sources.

Formally, we define our observations for the ICA as:

$$O(f, t) = L(d(t), f) - \sum_{i=1}^{N} l(D_i, f) = \sum_{i=1}^{N} l'(D_i, f)\delta_i(t). \tag{7}$$

As described above, these observations are linear combinations of the source signals. We can therefore use ICA to separate the source signals.

5 DEEPBREATH

DeepBreath is the first RF-based full night breathing reconstruction system that can accurately monitor multiple people even when they share the same bed. The breathing signals extracted by DeepBreath can be directly analyzed to learn the health status of the individuals, or fed to a sleep analysis system like the one described in [49].

DeepBreath runs on top of an FMCW radio equipped with an antenna array. The radio transmits a low power wireless signal and captures its reflections from users in the vicinity. Multi-antenna FMCW radios allow us to

capture the RF signal from a particular location in space [23] – i.e., they allow us to obtain multiple concurrent RF signals, each corresponding to the signal reflected from a particular voxel in space. We use this property to focus on RF signals from voxels in and around the bed. Each such RF signal is a mixture of the original breathing signals. We call such mixtures, "observations". The difference between observations stems from differences in the contribution of each breathing signal to that particular observation, which depends on the position of the person and the location that the observation focuses on.

DeepBreath takes as input a set of full-night observations and returns the breathing signals of each person. It does so by following a three-step process illustrated in Fig. 4 and summarized below:

- *Motion Detection:* The motion detection component takes as input observations, identifies motion intervals, and splits the observations into a series of stable periods, as shown in the first row of Fig. 4.
- *Breathing Separation:* This module processes the observations during each stable period to disentangle the breathing signals of different people. It outputs the reconstructed breathing signals during that period, as shown in the second row of Fig. 4.
- *Identity Matching:* The breathing separation module is not aware whom each reconstructed signal belongs to. In order to create full-night reconstruction, DeepBreath has a special module that stitches all reconstructed breathing signals that belong to the same person, as shown in the third row of Fig. 4.

Below we describe these components in detail.

5.1 Robust Human Motion Detector

When there are large motions, ICA will fail for two reasons. First, the frequency response of a large motion can no longer be approximated by the first order Taylor expansion, therefore its corresponding observations are no longer linear related to each other. Second, a large motion usually represents a change of posture of the user. He may move slightly away from his original position, and cause a change in the signal mixing pattern. Therefore, we should segment the signal when we detect large motions and apply ICA to each stable period separately.

Ideally, we want a motion detector that raises a flag only when one of the people moves but ignores other sources of motion. This is because only a movement of one of the breathing people disrupts the ICA. Other sources of motion in the environment (e.g., the HVAC) do not affect the contribution of each breathing signal to the observations.

To distinguish movements of the monitored individuals from other sources of motion, we rely on the following intuition. When one of the monitored people moves, the motion affects the breathing signal in every observation. On the contrary, environmental motions are usually further away from the person and they affect the breathing signal due to the sinc effect. Thus when an environmental motion occurs, the breathing pattern will be detectable in some observations.

In order to utilize the above intuition, we define the following terms:

Definition 5.1. **Short Observation** A short observation is a small period of a observation with a fixed duration.

We assume that the human's breathing rate is constant during a short period. This means that breathing can be assumed periodic during a short observation. Therefore, the periodicity of a short observation can represent its signal quality. Then we have:

Definition 5.2. **Short term Breathing-to-Noise Ratio (s-BNR)** $\mathcal{B}_s$ of a short observation o is defined as the ratio of breathing energy to the overall energy in observation o.

We computed B_s by first taking an FFT of the short observation signal. We then find the FFT bin with maximal energy within the human breathing range. We compute the ratio between that bin's energy and the energy sum of all FFT bins. In our computation, we use 15 seconds for the default duration of short observations and 10 to
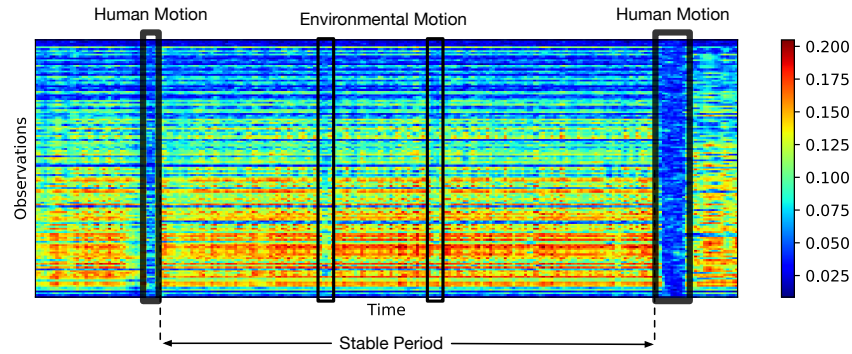
Fig. 5. An example of Motion Tableau. More reddish the cell is, higher the s-BNR of that short observation is. During this period, we can see three typical patterns. When there are no motion, a large part of short observations have high s-BNR. When there are environmental motions, some observations are affected, but there still exists high s-BNR observations. And when there are human motions, nearly all observations are destroyed. We call the period between two human motions as a stable period.

30 breaths/minute for the human breathing range [13, 32]. The larger the s-BNR, the more periodic the short observation is, then more likely the short observation contains good breathing signal.

Thus, an observation is a time series of short (15-second) observations, each of which has a particular B_s. Next, we define "a motion tableau" over all observations as follows:

Definition 5.3. **Motion Tableau** is a matrix with columns representing discretized time slots and rows representing observations at different locations. Each (i, j) cell represents the short observation at the jth location during ith time slot. The value of cell (i, j) is the s-BNR of that short observation.

Figure 5 shows an example of motion tableau computed over a full night of sleep of a couple in our dataset. The figure shows that the motion tableau has the following desirable property: Different kinds of motion have different patterns. Human motion usually causes all short observations during that period to have low s-BNR, whereas environmental motion does not affect the s-BNR much.

Then, instead of using hand-crafted features that are hard to tune, we can treat the motion tableau as an image and train a Convolutional Neural Network(CNN) based classifier to detect human motion. CNNs are well-known for its good accuracy and robustness on image classification tasks. Here, we adopt a classic VGG16 [35] architecture with adjustment of the input size and output dimension. The CNN classifies each column in the motion tableau to identify whether it experiences human motion. To classify the ith column, we feed the CNN a small image that includes all rows and the columns $[i - k, i + k]$, where k is a small number that allows the CNN to look at the context around the particular column of interest. The CNN outputs "one" to indicate movements of the monitored people and "zero" otherwise.

5.2 Breathing Separation

After motion detection, we can divide a single night into a series of stable periods. Ideally, we can apply ICA to each stable period and obtain the breathing reconstructions. Yet, there are still two practical challenges:

(1) The direct path of the farther person may be completely blocked. Thus, we cannot assume breathing signals are always located in the bed area.

(2) Noise may completely overwhelm breathing signals in some observations. Such observations no longer satisfy the linearity property and are harmful to the reconstruction.

Therefore we propose a breathing quality filter to address both challenges.

5.2.1 Dealing with Blockage. To solve the blockage problem, we leverage a well-known phenomenon called multipath. Wireless signals can be reflected by walls and furniture, and can reach the receiver even though the direct path is not available. Fig. 6 shows a typical example. Although multipath signals have a different time-of-flight compared to the direct path signal, they are all linearly related to the origin breathing motion. Therefore, multipath signals provide the same level of information as direct path signals. So, instead of only focusing on bed area, we use observations from the larger space around the bed to gather as much information as possible.
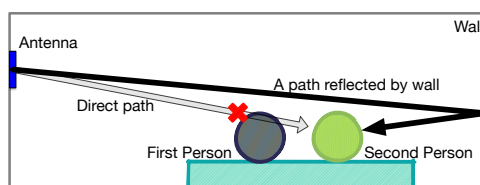

Fig. 6. A multipath example. The direct path from the device to the second person is blocked by the first person. Yet the second person can be reached by signals reflected by a wall.

5.2.2 Filtering Noisy Observations. As explained earlier, we need to consider observations in the larger area around the bed, so that we may recover the breathing of a person whose direct path to the receiver is occluded. On the other hand, for observations that are located far away from the person, the breathing signals will be suppressed and noise will become the main component. Feeding such noisy observations to ICA is harmful since ICA will then try to reconstruct the noise pattern.

To filter out noisy observations and keep the useful ones, we again rely on the periodicity of human breathing. Specifically, a good observation should have many short observations (sequences of 15 seconds) that exhibit high s-BNR. Thus, we propose the following definition to measure the signal quality during long observation, i.e. the observation over a whole stable period:

Definition 5.4. **Long term Breathing-to-Noise Ratio (l-BNR)** $\mathcal{B}_l$ of a long observation o is computed as the average of the s-BNR of the series of short observations that constitute the long observation.

A low l-BNR indicates a low possibility that the observation contains useful breathing information, and hence such observations should not excluded in recovering breathing signals. Once we filter out such low l-BNR observations, we can apply our model introduced in section 4 and reconstruct the breathing signals of the people in the scene.

5.3 Identity Matching

After we apply the breathing separation algorithm to each stable period, we get several ICA components for each of them. Assuming, in each stable period, that the ICA components are all successfully reconstructed breathing signals, the last step to get the full night breathing of every person is to figure out which ICA component corresponds to which person. We call this problem, *identity matching*.

Identity matching is non-trivial even in the case of two people. Say we have two people p_1 and p_2. In each stable period, we have two ICA components c_1, c_2. There are two choices when matching these components: c_1 is p_1's

Table 1. All key notations

Symbol	Meaning
N	number of people
M	number of stable periods
K	number of ICA components in each stable periods
p_n	nth person ($n = 1, .., N$)
q_m	mth stable periods ($m = 1, .., M$)
c_m^k	kth ICA component in stable period q_m ($k = 1, .., K$)
$\mathcal{M}(c_m^k)$	mixing vector of ICA components c_m^k
$\mathcal{M}(c_m^k)_i$	ith element in mixing vector $\mathcal{M}(c_m^k)$
$\mathcal{I}(\cdot, \cdot)$	identity consistency metric for two ICA components
$\mathcal{I}_\sigma(\cdot, \cdot)$	identity consistency metric for two ICA assignments
$\sigma_m : \{1, .., N\} \rightarrow \{1, .., K\}$	ICA assignment in stable periods q_m

breathing, c_2 is p_2's breathing or vice versa. One now needs to make such a choice for each stable period. Because we have at least two possible matchings in each stable period, the valid solution space grows exponentially with the number of stable periods. Things can become much more complex when the number of people or the number of ICA components are larger than two.

To solve the identity matching problem, we start by defining a consistency metric that captures the likelihood that two ICA components represent the breathing signal of the same person. We then formulate identity matching as an optimization problem that assigns identities to maximize the consistency metric. We show how to solve the optimization problem efficiently using dynamic programming. We explain this process in detail below. Table 1 summarizes the notations used this section.

5.3.1 Identity Consistency Metric. We define an identity consistency metric $\mathcal{I}$. Metric $\mathcal{I}$ takes two ICA components c_1, c_2 (from different stable periods) as input, and gives a consistency score $\mathcal{I}(c_1, c_2)$ as output. The higher the consistency score, $\mathcal{I}(c_1, c_2)$ is, the more likely the ICA components c_1, c_2 are the breathing of the same person during two stable periods.

To compute $\mathcal{I}$ we leverage the mixing vector of the ICA components. The mixing vector $\mathcal{M}(c)$ is one column of the mixing matrix (W in section 4) that corresponds to ICA component c. The length of the mixing vector is the number of original observations we used to generate the ICA components. Each entry of the mixing vector represents how this ICA component c contributes to its corresponding observation. Two ICA components having similar mixing vectors means that they contribute similarly to the RF observations. Thus they are more likely to represent the same source signal.[4]

Then we mathematically define the ICA component identity consistency metric $\mathcal{I}$ as follows:

$$\mathcal{I}(c_1, c_2) = \sum_i \frac{\min(\mathcal{M}(c_1)_i, \mathcal{M}(c_2)_i)}{\max(\mathcal{M}(c_1)_i, \mathcal{M}(c_2)_i)} \tag{8}$$

where the index i runs over all the entries of the corresponding mixing vectors.

5.3.2 Consistent Identity Assignments. We introduce the ICA assignment σ_m for stable periods q_m. Each assignment can be viewed as a permutation of the ICA components. Specifically, $\sigma_m(n) = k$ means ICA component c_m^k is assigned as person p_n's breathing in ICA assignment σ_m.

---

[4]Note that since ICA is not sensitive to scale, mixing vectors of different ICA components may have different scales. Thus before doing comparison, we have to normalize the mixing vectors.

We compute the consistency score of two assignments for two stable periods by computing the consistency between the components they assign to the same person, as follows:

$$\mathcal{I}_\sigma(\sigma_m, \sigma_{m'}) \triangleq \sum_{n=1}^{N} \mathcal{I}(c_m^{\sigma_m(n)}, c_{m'}^{\sigma_{m'}(n)}), \tag{9}$$

where the sum is over all people and $\mathcal{I}(c_m^{\sigma_m(n)}, c_{m'}^{\sigma_{m'}(n)})$ is the consistency between a pair of ICA components that were assigned the same identity by assignments σ_m and $\sigma_{m'}$.

The score $\mathcal{I}_\sigma(\sigma_m, \sigma_{m'})$ is used to measure whether ICA assignment σ_m and $\sigma_{m'}$ reorder the ICA components in a *consistent* way. By saying *consistent*, we mean that after the reordering, ICA components having the same order in two stable periods do actually represent the breathing of the same person.

5.3.3 Objective Function and Solution. Our goal is to find ICA assignments σ_m for each stable periods such that after reordering, an ICA component having the same order in all stable periods is the same person's breathing. Thus, we define the following objective function $\mathcal{J}$.

$$\mathcal{J}(\sigma_1, .., \sigma_M) = \sum_{m=1}^{M} \sum_{m'=m+1}^{\min(M, m+h)} \mathcal{I}_\sigma(\sigma_m, \sigma_{m'}) \tag{10}$$

The objective $\mathcal{J}$ simply sums all the ICA assignment identity consistency scores for all pairs of ICA assignments in two different and *temporally close* stable periods. Here, two stable periods $q_m, q_{m'}$ are considered as *temporally close* if there are less than h stable periods between these two stable periods .i.e $|m - m'| \le h$ (our default is h=12). The reason why we limit ourselves to nearby stable periods is that the consistency metric I is valid only over a short period. Specifically, the consistency metric captures the fact that when a person tosses around in bed, or moves on a chair or couch, he is still in the same general location and hence the mixing matrix of his breathing changed by a small amount. However, if the person keeps moving, then eventually the mixing matrix can change significantly.

The above objective function captures the idea that if each pair of ICA assignments orders ICA components in a consistent way then all the ICA assignments order the ICA components consistently. Thus, the optimal set of assignments can be represented as:

$$\sigma_1^*, .., \sigma_M^* = \arg\max \mathcal{J}(\sigma_1, .., \sigma_M) \tag{11}$$

To solve the optimization in Eq.(11), we design a dynamic programming algorithm which performs two passes, forward and backward. In the forward pass, we have initial conditions f_h and DP-equation f_m and g_m as follow:

$$f_h(\sigma_1, .., \sigma_h) = \sum_{i=1}^{h} \sum_{j=i+1}^{h} \mathcal{I}_\sigma(\sigma_i, \sigma_j) \tag{12}$$

$$f_m(\sigma_{m-h+1}, .., \sigma_m) = \max_{\sigma_{m-h}} f_{m-1}(\sigma_{m-h}, .., \sigma_{m-1}) + \mathcal{I}_\sigma(\sigma_{m-h}, \sigma_m), \quad m = h+1, h+2, .., M \tag{13}$$

$$g_m(\sigma_{m-h+1}, .., \sigma_m) = \arg\max_{\sigma_{m-h}} f_{m-1}(\sigma_{m-h}, .., \sigma_{m-1}) + \mathcal{I}_\sigma(\sigma_{m-h}, \sigma_m), \quad m = h+1, h+2, .., M \tag{14}$$

In the backward pass, we can get optimal solution $\sigma_1^*, .., \sigma_M^*$ in a reverse order based on the DP-functions computed in forward pass.

$$\sigma_{M-h+1}^*, .., \sigma_M^* = \arg\max f_M(\sigma_{M-h+1}, .., \sigma_M) \tag{15}$$

$$\sigma_m^* = g_{m+h}(\sigma_{m+1}^*, .., \sigma_{m+h}^*), \quad m = M-h, M-h-1, .., 1 \tag{16}$$

(a) Signals captured from chest and diaphragm

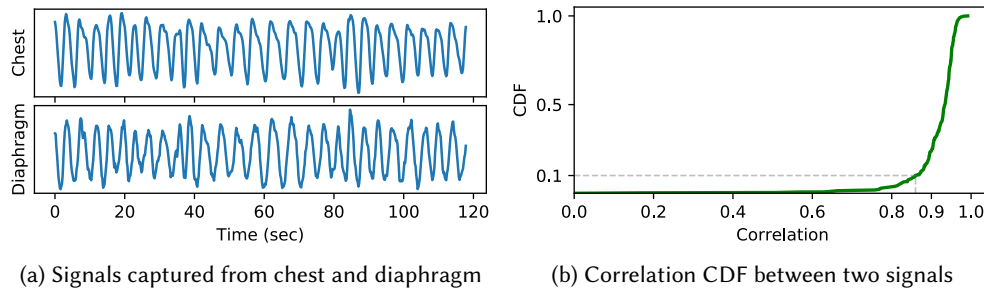(b) Correlation CDF between two signals

Fig. 7. Comparison between chest level and diaphragm level breathing signals. Fig. 7a shows a 2 minutes sample of two breathing signals, and Fig. 7b shows the the correlation CDF between two breathing signals.

6 EVALUATION

In this section, we empirically evaluate our theoretical model and DeepBreath's performance. All experiments with human subjects are approved by our IRB and we have obtained informed consent from every subject. For the hardware, we have implemented a state-of-art FMCW radio that sweeps from $5.7GHz$ to $7.2GHz$ and transmits at sub-milliwatt power in accordance with the FCC regulations. The radio is equipped with an antenna array to improve spacial resolution.

Ground Truth: To obtain the ground truth breathing of people, we use SleepView[36], an FDA-approved sleep and apnea monitor. The user sleeps while wearing a special belt that uses respiratory inductance plethysmography to measure the expansion of the chest, which it translates to breathing signal.

Metrics: To evaluate our breathing reconstruction results, we use the following two metrics:

- *Pearson correlation coefficient (correlation):* We evaluate the similarity between the reconstructed signal and the ground truth by computing their correlation. The correlation is computed over stable periods. The aggregate per-night correlation is computed by taking a weighted average of the correlation over stable periods where the weight corresponds to the length of each period (normalized by the total duration of stable periods throughout the night).

  The optimal value for the correlation is 1. This would happen if the reconstructed signal is exactly the same as the ground truth. Of course in practice, the correlation is never 1. Thus, it is natural to ask what correlation value is good enough. To answer this question we compare the correlation between two respiration belts on the same person: one is strapped around the chest and the other around the diaphragm area. Both belts capture the person's breathing but at slight different locations on the body. Fig. 7a plots an example that shows the breathing signal of the same person captured at the chest and diaphragm levels. The figure shows small differences between the two signals. For quantitative results, we plot in Fig. 7b a CDF of the the correlation between two breathing signals. The data in the figure are taken over 2-minute windows from 6 individuals over 6 nights. As can be seen from the figure, the two breathing signals are slightly different –i.e. their correlation is not 1. The average correlation is 0.915 and 90th percentile is 0.860. This CDF provides a point of comparison. Specifically, since the RF signal captures reflections from multiple areas of the human body, an ideal reconstruction would show a correlation comparable to the correlation between the breathing signals captured in different locations on the body.

- *Breathing Rate:* Breathing rate is the number of breaths per minute. We compare our reconstructed signal to the ground truth breathing rate as captured by the respiration belt. As in past work, we compute the breathing rate over 2-minute windows.
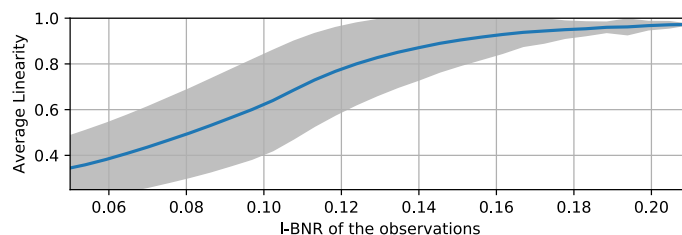
Fig. 8. Linearity of an observation as a function of its l-BNR. Blue line represents the average linearity of observations with certain l-BNR and grey area shows the standard deviation. The figure shows that observations with high l-BNR are linear functions of the breathing signals.

6.1 Empirical Validation of Our Model

The use of ICA to separate mixed signals is subject to three requirements: 1) the mixing is linear, 2) the sources are independent, and 3) the distributions of the source signals are not Gaussian.

We empirically check that our formulation of the breathing separation problem satisfies all three requirements. We conduct an experiment in which two people sit shoulder-to-shoulder on a couch. Each subject is asked to wear a breathing belt to record his ground-truth breathing signal. The subjects breathe normally with no restrictions. Each trial lasts for 5 minutes. In total, we invite 10 people to participate in this experiment and conduct 20 trials.

(a) Linearity of the Observations: To check whether the observations are linear combinations of breathing signals, we measure the *linearity* of a given observation $O(t)$ as follows:

$$l_O = \max_{a_1, a_2} |\rho(a_1 s_1(t) + a_2 s_2(t), O(t))|, \tag{17}$$

where $s_1(t)$ and $s_2(t)$ are the ground truth breathing signals, $O(t)$ is the observation signal, and $\rho()$ is the Pearson correlation coefficient function. This metric computes the correlation between the observation and the closest linear combination of the signals.

We plot in Fig. 8 the linearity of observations as a function of their l-BNR. The figure shows that the linearity of an observation increases with l-BNR. This is expected because observations with low l-BNR are dominated by noise. The figure also shows that when the l-BNR is higher than 0.15, linearity is higher than 0.9. Thus, we can treat high l-BNR observations as linear functions of the breathing signals.

(b) Independence of the Source: Second, we examine the correlation between the breathing of two subjects as a function of the duration of an observation. For each duration t, we divide the duration of the experiment to non-overlap periods of length t. For each such period, we compute the correlation between the breathing of the two subjects in the experiment. We repeat this computation for all subjects and trials. Fig. 9 plots the relationship between the correlation of the subject's ground-truth breathing and the duration of the observation. The blue line represents the averaged correlation, and the grey area shows the standard deviation. The figure shows that the correlation of the subjects breathing signals decreases as the duration of the observation increases, and is lower than 0.1 when the duration is larger than 2 minutes. Thus, it is safe to assume that the breathing signals of different subjects are statistically independent over periods equal or larger than two minutes.[5]

(c) Non-Gaussianity of the Sources: Finally, we look at the distribution of the breathing signals of our subjects. We show a representative example of the ground truth breathing of a subject in Fig. 10a and its distribution in Fig. 10b. Clearly the distribution is not Gaussian. The distributions of other subjects are similarly non-Gaussian.

---

[5]Note that two signals can look similar but still have low correlation if the frequency of breathing is slight different or the breathing cycles are unsynchronized.
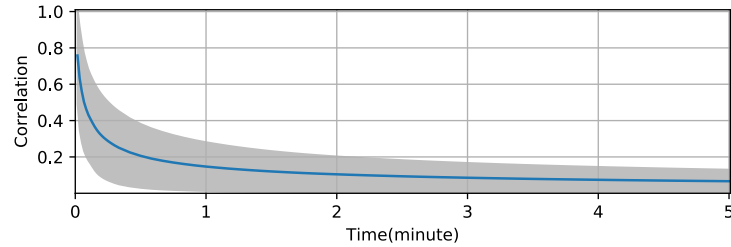
Fig. 9. Correlation between the breathing of two subjects over windows with different duration. Blue line represents the average correlation between subjects and and grey area shows the standard deviation.
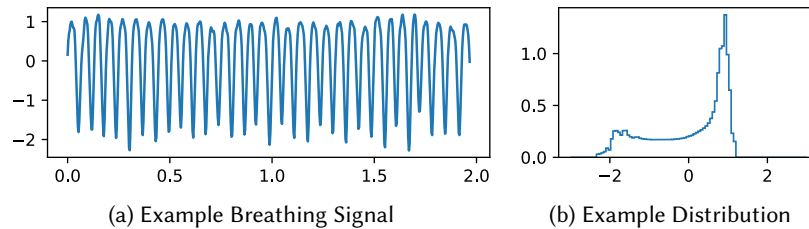

(a) Example Breathing Signal   (b) Example Distribution

Fig. 10. Figure shows that marginal distribution of a subject breathing is non-Gaussian

6.2 Evaluation of DeepBreath's Performance

We deploy our system and evaluate it with 13 different couples. The experiments are run in the couple's own homes. All monitored couples sleep in the same bed. The bed size ranges from twin ($1m$ wide) to king ($2m$). Each subject wears a breathing belt for the whole night to obtain the ground truth breathing. We install our device at the bedside. We refer to the subject who sleeps closer to the device as the *near* subject and the other subject as the *far* subject. In total, we have collected 21 nights, and 151 hours of data.

We first generate stable periods for each night by detecting all motion using the motion detector. We remove periods with motion and operate on stable periods. Our analysis shows that, on average, 11% of a night exhibits motion. This is compatible with medical literature [10].[6] We then process the stable periods and compare them with the ground truth breathing signals.

We also compare the performance of DeepBreath with a baseline that uses an oracle to iterate over all voxels in the bed area, and for each person, it zooms in on the voxel that results in the most accurate breathing signal for that person. This baseline highlights the importance of disentangling the breathing signals as opposed to zooming in on the best RF signal that corresponds to the person's breathing, as in past work. Note that the baseline is a conservative representation of past work since we allow it to look at the actual ground truth breathing as it picks the best signal.

Fig. 11a plots a CDF of the correlation between the reconstructed breathing signals and the ground truth for both DeepBreath and the baseline. The figure shows that DeepBreath's average correlation is 0.920 and 0.908 for the near and far subjects respectively. This is comparable with the average correlation between two belts that capture breathing at two locations on the same person. In comparison, the baseline achieves a correlation of 0.874 and 0.733 for the near and far subjects respectively. This performance is significantly worse than DeepBreath's,

---

[6]Healthy people experience around 30 minutes of intermittent awakenings each night [10]. Since we monitor a couple, we detect motion when either of them moves.

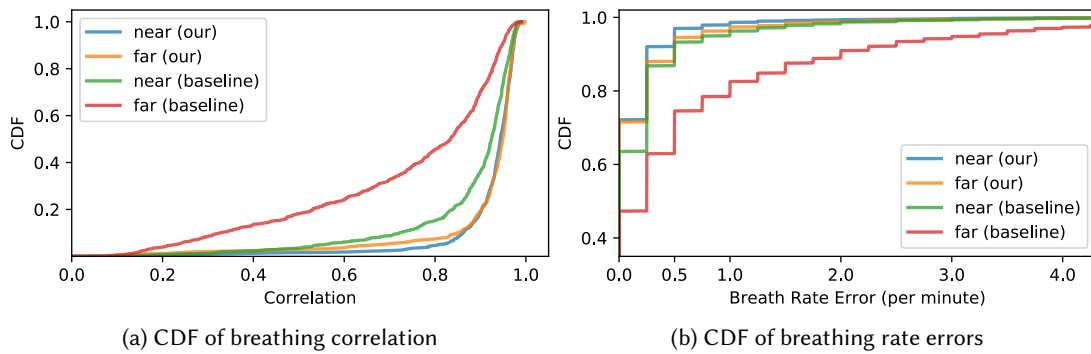(a) CDF of breathing correlation   (b) CDF of breathing rate errors

Fig. 11. Performance comparison between DeepBreath and an oracle-based baseline.

particularly for the far person. Note that, as mentioned earlier, the baseline is allowed to look at the ground truth signals so that it can zoom in on the RF signals with the best correlation, which is not feasible in practice. Despite this extra information, it is still unable to match DeepBreath's performance.

Fig. 11b plots a CDF of the error in estimating the breathing rate for both DeepBreath and the baseline. The median breathing rate error in DeepBreath is 0.121 and 0.158 for the near and far subjects. In contrast, the baseline shows a breathing rate error of 0.200 and 0.633 for the near and far subjects respectively.

There are two reasons for the lower performance of the baseline. First, for most cases, since the subjects are fairly close, their breathing signals are mixed in all locations in space. Thus, sometimes it is not possible to find a good voxel that includes breathing from only one subject. Second, the signal from the near person can be much stronger than the far person, and the body of the near person can sometimes occlude the body of the far person. DeepBreath does not suffer from these problems because it is intrinsically designed to separate mixed signals. Further, it combines information across all observations and can leverage multipath effects to reconstruct the breathing of the far person.

Finally, Fig. 12 shows a few examples of our reconstructed breathing signals and the corresponding ground truth signals. The figure shows that DeepBreath is able to separate a coupleâĂŹs respiration signals even when their breathing patterns look similar. It also shows that DeepBreath can deal with irregular breathing patterns such as those experienced by the far person in couple 2 and couple 3.

7 EVALUATION OF THE COMPONENTS OF DEEPBREATH

The above result shows that DeepBreath can correctly recover the breathing of each individual even when they share the bed. In this section, we zoom in on the identity matching and motion detection components to understand their performance.

Evaluation of Identity Matching: We report the accuracy of identity matching for all stable periods in the collected 21 nights. We compute the average accuracy weighted by the duration of each stable period. The total averaged accuracy is 99.1% and accuracy for each subject is shown in Fig. 13. Accuracies of all the subjects are above 95%, which shows the robustness of our identity matching algorithm.

Evaluation of Motion Detection: We also evaluate the motion detection component. To obtain the ground truth motion we have asked 4 subjects to sleep while wearing accelerometers on each ankle and each wrist. In this experiment, each subject sleeps in a separate bed to ensure that the motion captured by the accelerometers is as close to the ground truth as possible. Each subject also wears a breathing belt for ground truth breathing.
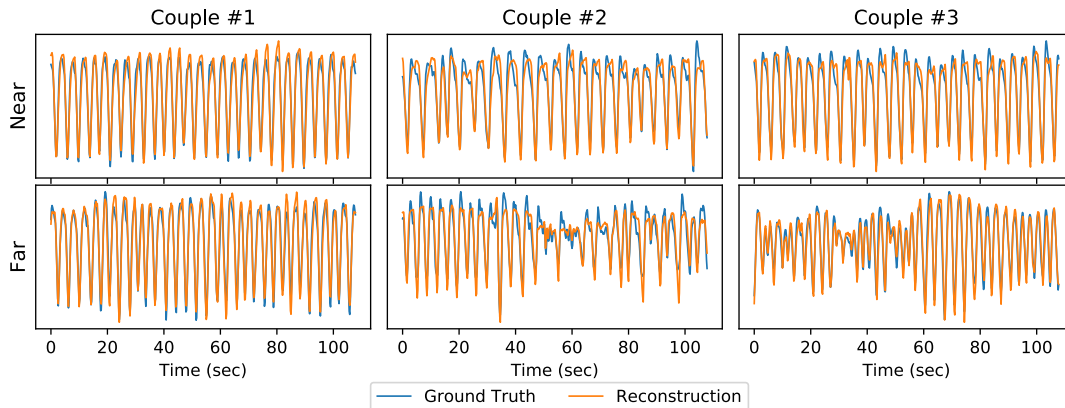
Fig. 12. Examples of recovered breathing signals and the original ground truth signals from the breathing belt. The figure shows that DeepBreath is accurate even when the monitored couple have similar breathing rates or their breathing signals have irregular patterns.
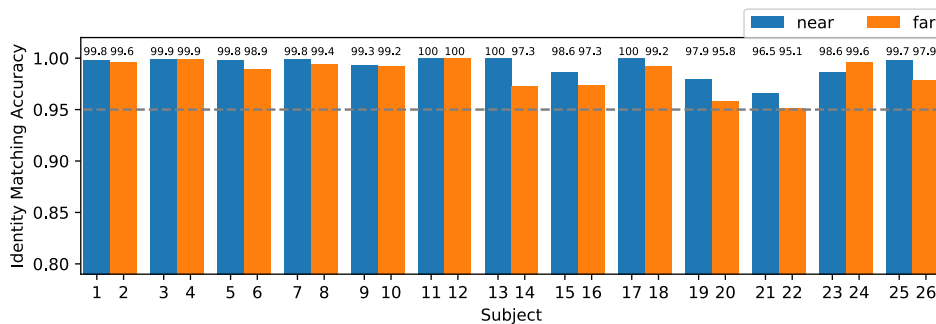

Fig. 13. Accuracy of identity matching. Each bar shows the identity matching accuracy of each subject.

Accelerometers are affected by gravity. To eliminate this effect we subtract the average acceleration and consider only changes. Because the reading from the accelerometer is noisy, for each 30 second period, we say there is a human motion if the acceleration is 2 times larger than the standard deviation. We declare motion if any accelerometer experiences a motion event. We compare the output of our motion detector to the result of predicting motion based on the four accelerometers. On average we achieve a precision of 0.933 and a recall of 0.954. This result shows that our motion detector successfully detects motion.

7.1 Breathing Separation with Many People

Finally, we would like to show that DeepBreath is not limited to two people and can scale to a larger number of users. We conduct an experiment with 5 subjects sitting shoulder-to-shoulder on a 1.9m couch, as shown in Fig. 14. The subjects wear a breathing belt to capture the ground truth breathing signals. In total we invited 8 people to participate in this experiment, and we conducted 3 trials with different subject combinations. Each trial lasts for 5 minutes.

Fig. 14. Experiment setup. 5 subjects are sitting shoulder-to-shoulder on a 1.9*m* couch.

(a) Observations at each subject's location

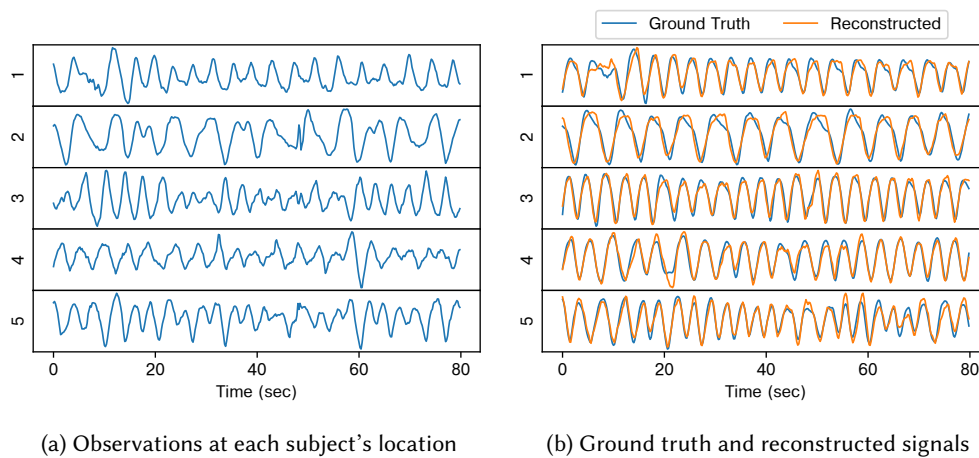(b) Ground truth and reconstructed signals

Fig. 15. Five people experiment. Observations at each subject's location are plotted in Fig. 15a. Because there are no gaps between subjects, breathing signals are mixed together. But DeepBreath can reconstruct the breathing of each subject accurately, as shown in Fig. 15b, with an average correlation of 0.92.

Fig. 15a shows the observations at the voxels centered on each of the five subjects. Each observation is a different mixture of the breathing signals of the subjects. Fig. 15b plots the ground truth and the reconstructed breathing signals. As can be seen, even though every observation is a mixture of multiple subject's breathing, our algorithm can still reconstruct the breathing of each subject accurately. On average, we achieve 0.922 correlation and 0.034 breathing rate error with respect to the ground truth breathing signals. These results demonstrate that DeepBreath can reconstruct the breathing of at least 5 people even when there is nearly zero distance between them.

8 CONCLUSION

We present DeepBreath, the first wireless system that disentangles breathing signals of multiple individuals from mixtures of such signals. As a result, it can provide contactless respiration monitoring of multiple people even when they have zero distance between them. A user study with 13 couples who used DeepBreath for 21 nights in their own homes shows that DeepBreath is highly accurate.

We believe DeepBreath opens the door for contactless multi-person sleep studies. Its output can directly serve as the input for sleep stage classifiers [22, 49], or apnea detectors [3, 42]. As such it extends the benefits of such contactless monitoring to couples and individuals sharing the same bed.

In this paper, we have focused on mixtures of breathing signals. However, the model and system components that we developed extend beyond breathing to other small motions that modulate FMCW signals. Future work will examine applications to disentangle other types of motion, e.g., typing, or the simultaneous motion of two hands.

ACKNOWLEDGMENTS

REFERENCES

[1] Fadel Adib, Zachary Kabelac, Dina Katabi, and Robert C Miller. 2014. 3D Tracking via Body Radio Reflections.. In *NSDI*.
[2] Fadel Adib, Hongzi Mao, Zachary Kabelac, Dina Katabi, and Robert C Miller. 2015. Smart homes that monitor breathing and heart rate. In *CHI*.
[3] Laiali Almazaydeh, Khaled Elleithy, Miad Faezipour, and Ahmad Abushakra. 2013. Apnea detection based on respiratory signal classification. *Procedia Computer Science* (2013).
[4] Richard B Berry, Rohit Budhiraja, Daniel J Gottlieb, David Gozal, Conrad Iber, Vishesh K Kapur, Carole L Marcus, Reena Mehra, and others. 2012. Rules for scoring respiratory events in sleep: update of the 2007 AASM manual for the scoring of sleep and associated events: deliberations of the sleep apnea definitions task force of the American Academy of Sleep Medicine. *JCSM* (2012).
[5] Bosch 2018. https://www.boschtools.com/us/en/boschtools-ocs/laser-measuring-glm-50-35087-p/. (2018).
[6] Mary A Carskadon, William C Dement, and others. 2005. Normal human sleep: an overview. *Principles and practice of sleep medicine* (2005).
[7] Ashish Chaddha. 2015. Slow breathing and cardiovascular disease. *International journal of yoga* (2015).
[8] Seungjin Choi, Andrzej Cichocki, Hyung-Min Park, and Soo-Young Lee. 2005. Blind source separation and independent component analysis: A review. *Neural Information Processing-Letters and Reviews* (2005).
[9] Sergei Churkin and Lesya Anishchenko. 2015. Millimeter-wave radar for vital signs monitoring. In *COMCAS*. IEEE.
[10] Luciane de Souza, Ana Amélia Benedito-Silva, Maria Laura Nogueira Pires, Dalva Poyares, Sergio Tufik, and Helena Maria Calil. 2003. Further validation of actigraphy for sleep studies. *Sleep* (2003).
[11] Arnaud Delorme and Scott Makeig. 2004. EEGLAB: an open source toolbox for analysis of single-trial EEG dynamics including independent component analysis. *Journal of neuroscience methods* (2004).
[12] WW Flemons, D Buysse, S Redline, A Oack, K Strohl, J Wheatley, T Young, N Douglas, P Levy, W McNicolas, and others. 1999. Sleep-related breathing disorders in adults: recommendations for syndrome definition and measurement techniques in clinical research. *Sleep* (1999).
[13] William F Ganong and William Ganong. 1995. *Review of medical physiology*. Appleton & Lange Norwalk, CT.
[14] Chen-Yu Hsu, Aayush Ahuja, Shichao Yue, Rumen Hristov, Zachary Kabelac, and Dina Katabi. 2017. Zero-Effort In-Home Sleep and Insomnia Monitoring using Radio Signals. *IMWUT* (2017).
[15] Chen-Yu Hsu, Yuchen Liu, Zachary Kabelac, Rumen Hristov, Dina Katabi, and Christine Liu. 2017. Extracting Gait Velocity and Stride Length from Surrounding Radio Signals. In *CHI*. ACM.
[16] Aapo Hyvärinen, Juha Karhunen, and Erkki Oja. 2004. *Independent component analysis*. John Wiley & Sons.
[17] Aapo Hyvärinen and Erkki Oja. 2000. Independent component analysis: algorithms and applications. *Neural networks* (2000).
[18] Swarun Kumar, Stephanie Gil, Dina Katabi, and Daniela Rus. 2014. Accurate indoor localization with zero start-up cost. In *MobiCom*. ACM.
[19] Mark E Kunik, Kent Roundy, Connie Veazey, Julianne Souchek, Peter Richardson, Nelda P Wray, and Melinda A Stanley. 2005. Surprisingly high prevalence of anxiety and depression in chronic breathing disorders. *Chest* (2005).

[20] Ronald Ley. 1994. Breathing and the psychology of emotion, cognition, and behavior. In *Behavioral and psychological approaches to breathing disorders*.

[21] Xuefeng Liu, Jiannong Cao, Shaojie Tang, and Jiaqi Wen. 2014. Wi-Sleep: Contactless sleep monitoring via WiFi signals. In *RTSS*. IEEE.

[22] Xi Long, Jie Yang, Tim Weysen, Reinder Haakma, Jérôme Foussier, Pedro Fonseca, and Ronald M Aarts. 2014. Measuring dissimilarity between respiratory effort signals based on uniform scaling for sleep staging. *Physiological measurement* (2014).

[23] Bassem R Mahafza. 2002. *Radar systems analysis and design using MATLAB*. CBC Press.

[24] Nikolaos Mitianoudis and Tania Stathaki. 2007. Pixel-based and region-based image fusion schemes using ICA bases. *Information Fusion* (2007).

[25] Ken Monahan, Amy Storfer-Isser, Reena Mehra, Eyal Shahar, Murray Mittleman, Jeff Rottman, Naresh Punjabi, Mark Sanders, Stuart F Quan, Helaine Resnick, and others. 2009. Triggering of nocturnal arrhythmias by sleep-disordered breathing events. *Journal of the American College of Cardiology* (2009).

[26] Rajalakshmi Nandakumar, Shyamnath Gollakota, and Nathaniel Watson. 2015. Contactless sleep apnea detection on smartphones. In *MobiSys*. ACM.

[27] F Javier Nieto, Terry B Young, Bonnie K Lind, Eyal Shahar, Jonathan M Samet, Susan Redline, Ralph B D'agostino, Anne B Newman, Michael D Lebowitz, Thomas G Pickering, and others. 2000. Association of sleep-disordered breathing, sleep apnea, and hypertension in a large community-based study. *Jama* (2000).

[28] Erkki Oja. 2004. Applications of independent component analysis. In *International Conference on Neural Information Processing*. Springer.

[29] Kurt Peek. 2011. *Estimation and compensation of frequency sweep nonlinearity in FMCW radar*. Master's thesis. University of Twente.

[30] Pulmonology 2018. https://www.columbiamemorialhealth.org/pulmonology/. (2018).

[31] Tauhidur Rahman, Alexander T Adams, Ruth Vinisha Ravichandran, Mi Zhang, Shwetak N Patel, Julie A Kientz, and Tanzeem Choudhury. 2015. Dopplesleep: A contactless unobtrusive sleep sensing system using short-range doppler radar. In *UbiComp*. ACM.

[32] Alejandro Rodríguez-Molinero, Leire Narvaiza, Jorge Ruiz, and César Gálvez-Barrón. 2013. Normal respiratory rate and peripheral blood oxygen saturation in the elderly population. *Journal of the American Geriatrics Society* (2013).

[33] Hiroshi Saruwatari, Satoshi Kurita, and Kazuya Takeda. 2001. Blind source separation combining frequency-domain ICA and beamforming. In *ICASSP*. IEEE.

[34] Nandakumar Selvaraj. 2015. Psychological acute stress measurement using a wireless adhesive biosensor. In *EMBC*. IEEE.

[35] Karen Simonyan and Andrew Zisserman. 2014. Very deep convolutional networks for large-scale image recognition. *arXiv preprint* (2014).

[36] Sleepview 2018. https://clevemed.com/sleepview/. (2018).

[37] Frederick Snyder, J Allan Hobson, Donald F Morrison, and Frederick Goldfrank. 1964. Changes in respiration, heart rate, and systolic blood pressure in human sleep. *Journal of Applied Physiology* (1964).

[38] Tania Stathaki. 2011. *Image fusion: algorithms and applications*. Elsevier.

[39] Yu Takahashi, Tomoya Takatani, Keiichi Osako, Hiroshi Saruwatari, and Kiyohiro Shikano. 2009. Blind spatial subtraction array for speech enhancement in noisy environment. *IEEE transactions on audio, speech, and language processing* (2009).

[40] Alexander Tataraidze, Lesya Anishchenko, Lyudmila Korostovtseva, Bert Jan Kooij, Mikhail Bochkarev, and Yurii Sviryaev. 2015. Sleep stage classification based on respiratory signal. In *EMBC*. IEEE.

[41] Wang Tianben, Daqing Zhang, Yuanqing Zheng, Tao Gu, Xingshe Zhou, and Bernadette Dorizzi. 2017. C-FMCW Based Contactless Respiration Detection Using Acoustic Signal. In *IMWUT*.

[42] Péter Várady, Szabolcs Bongár, and Zoltán Benyó. 2003. Detection of airway obstructions and sleep apnea by analyzing the phase relation of respiration movement signals. *IEEE Transactions on Instrumentation and Measurement* (2003).

[43] Hao Wang, Daqing Zhang, Junyi Ma, Yasha Wang, Yuxiang Wang, Dan Wu, Tao Gu, and Bing Xie. 2016. Human respiration detection with commodity wifi devices: do user location and body orientation matter?. In *UbiComp*. ACM.

[44] Yang Xu, Wei Yang, Jianxin Wang, Xing Zhou, Hong Li, and Liusheng Huang. 2018. WiStep: Device-free Step Counting with WiFi Signals. *Proceedings of the ACM on Interactive, Mobile, Wearable and Ubiquitous Technologies* (2018).

[45] Zhicheng Yang, Parth H Pathak, Yunze Zeng, Xixi Liran, and Prasant Mohapatra. 2016. Monitoring vital signs using millimeter wave. In *Mobihoc*. ACM.

[46] Terry Young, Laurel Finn, Paul E Peppard, Mariana Szklo-Coxe, Diane Austin, F Javier Nieto, Robin Stubbs, and K Mae Hla. 2008. Sleep disordered breathing and mortality: eighteen-year follow-up of the Wisconsin sleep cohort. *Sleep* (2008).

[47] Terry Young, Paul Peppard, Mari Palta, K Mae Hla, Laurel Finn, Barbara Morgan, and James Skatrud. 1997. Population-based study of sleep-disordered breathing as a risk factor for hypertension. *Archives of internal medicine* (1997).

[48] Mingmin Zhao, Fadel Adib, and Dina Katabi. 2016. Emotion recognition using wireless signals. In *MobiCom*. ACM.

[49] Mingmin Zhao, Shichao Yue, Dina Katabi, Tommi S. Jaakkola, and Matt T. Bianchi. 2017. Learning Sleep Stages from Radio Signals: A Conditional Adversarial Architecture. In *ICML*.

APPENDIX A   EQUATION OF FMCW FREQUENCY RESPONSE

In this appendix we derive Eq. 3 from Eq. 2. For simplification, we use d to denote $d(t)$. Recall inside each sweep $u \in [0, T_s]$, with a reflector at distance d, the received FMCW signal can be written as:

$$m(d, u) = Ae^{j2\pi(F_0\tau(d)+K_s\tau(d)u-1/2K_s\tau(d)^2)}, u \in [0, T_s], \tag{18}$$

Because the signal travels with the speed of light, $\tau(d)^2$ is a small amount and can be ignored. Then we have:

$$m(d, u) \approx Ae^{j2\pi(F_0\tau(d)+K_s\tau(d)u)}, u \in [0, T_s] \tag{19}$$

Next we compute the frequency response of $m(d, u)$ at frequency f by applying continuous Fourier Transform.

$$l(d, f) = \int_0^{T_s} m(d, u)e^{-j2\pi fu}du = Ae^{j2\pi F_0\tau(d)} \int_0^{T_s} e^{j2\pi(K_s\tau(d)+f)u}du \tag{20}$$

Define $v(d, f) \triangleq T_s(K_s\tau(d) + f) = d/U + T_sf$, then we have:

$$l(d, f) = Ae^{j2\pi F_0\tau(d)} \int_0^{T_s} e^{j2\pi v(d,f)u/T_s}du \tag{21}$$

$$= Ae^{j2\pi F_0\tau(d)} \frac{e^{j2\pi v(d,f)u/T_s}\big|_{T_s} - e^{j2\pi v(d,f)u/T_s}\big|_0}{j2\pi v(d, f)/T_s} \tag{22}$$

$$= AT_se^{j2\pi F_0\tau(d)} \frac{e^{j2\pi v(d,f)} - 1}{j2\pi v(d, f)} \tag{23}$$

Noticing that

$$F_0\tau(d) = \frac{F_0}{B_w}(B_w\tau(d) + T_sf - T_sf) = R(d/U + T_sf) - RT_sf = Rv(d, f) - RT_sf \tag{24}$$

We can rewrite the Eq. 23 as following:

$$l(d, f) = AT_se^{-j2\pi RT_sf} \cdot e^{j2\pi Rv(d,f)} \frac{e^{j2\pi v(d,f)} - 1}{j2\pi v(d, f)} \tag{25}$$

Define $h(f) = AT_se^{-j2\pi RT_sf}$, then we have:

$$l(d, f) = h(f) \cdot e^{j2\pi Rv(d,f)} \frac{e^{j2\pi v(d,f)} - 1}{j2\pi v(d, f)} \tag{26}$$

Given the fact that

$$e^{j2x} - 1 = (\cos 2x - 1) + j\sin 2x = -2\sin^2 x + 2j(\sin x \cos x) \tag{27}$$

$$= 2\sin x(j\cos x - \sin x) = 2j\sin x(\cos x + j\sin x) = 2j\sin xe^{jx} \tag{28}$$

We have

$$l(d, f) = h(f) \cdot e^{j2\pi Rv(d,f)} \frac{2j\sin(\pi v(d, f))e^{j\pi v(d,f)}}{2j\pi v(d, f)} \tag{29}$$

$$= h(f) \cdot sinc(v(d, f)) \cdot e^{j2\pi(R+1/2)v(d,f)} \quad \blacksquare \tag{30}$$